

Hurricane risk assessment of offshore wind turbines

Spencer T. Hallowell ^{a,*}, Andrew T. Myers ^b, Sanjay R. Arwade ^a, Weichiang Pang ^c, Prashant Rawal ^c, Eric M. Hines ^d, Jerome F. Hajjar ^b, Chi Qiao ^b, Vahid Valamanesh ^e, Kai Wei ^f, Wytan Carswell ^g, Casey M. Fontana ^a

^a University of Massachusetts Amherst, USA

^b Northeastern University, USA

^c Clemson University, USA

^d Tufts University, USA

^e Risk Management Solutions, Newark, CA, USA

^f Southwest Jiaotong University, PR China

^g Haley & Aldrich, Inc, USA



ARTICLE INFO

Article history:

Available online 20 February 2018

Keywords:

Offshore wind
Risk
Hurricane
Fragility
Framework

ABSTRACT

A barrier to the development of the offshore wind resource along the U.S. Atlantic coast is a lack of quantitative measures of the risk to offshore wind turbines (OWTs) from hurricanes. The research presented in this paper quantifies the risk of failure of OWTs to hurricane-induced wind and waves by developing and implementing a risk assessment framework that is adapted from a well-established framework in performance-based earthquake engineering. Both frameworks involve the convolution of hazard intensity measures (IMs) with engineering demand parameters (EDPs) and damage measures (DMs) to estimate probabilities of damage or failure. The adapted framework in this study is implemented and applied to a hypothetical scenario wherein portions of nine existing Wind Farm Areas (WFAs), spanning the U.S. Atlantic coast, are populated with ~7000 5 MW OWTs supported by monopiles. The IMs of wind and wave are calculated with a catalog representing 100,000 years of simulated hurricane activity for the Atlantic basin, the EDPs are calculated with 24 1-h time history simulations, and a fragility function for DM is estimated by combining variability observed in over one hundred flexural tests of hollow circular tubes found in the literature. The results of the study are that, for hurricane-induced wind and wave, the mean lifetime (i.e., 20-year) probability of structural failure of the tower or monopile of OWTs installed within the nine WFAs along the U.S. Atlantic coast ranges between 7.3×10^{-10} and 3.4×10^{-4} for a functional yaw control system and between 1.5×10^{-7} and 1.6×10^{-3} for a non-functional yaw control system.

© 2018 Elsevier Ltd. All rights reserved.

1. Introduction

The offshore wind energy industry in the U.S. is poised for dramatic growth. The U.S., which currently has 30 MW of installed offshore wind capacity, has declared ambitious goals of installing 22,000 MW of offshore wind capacity by 2030, and 86,000 MW by 2050 [1]. To set these goals in context, the current worldwide capacity of offshore wind-generated power is ~10,000 MW, nearly all of which is generated in Northern Europe where the offshore wind industry has matured over the past few decades [1]. One major difference between the European and U.S. offshore environments is

the presence of hurricanes on the U.S. Gulf and Atlantic coasts. In the U.S., there are currently 33 wind energy areas, wind lease areas, and call areas designated by the U.S. Bureau of Ocean Energy Management, 21 of which are located along the Atlantic coast and therefore exposed to risk from hurricanes [2,3]. These areas are henceforth grouped together according to geographic proximity and referred to as Wind Farm Areas (WFAs). According to the archives of the National Hurricane Center (NHC), since 1900, there have been 33 hurricane tracks that have intersected the nine Atlantic WFAs and 62 that have passed within 50 km [2–4]. Recognizing this situation, the U.S. Department of Energy has advised that research should be conducted to better understand the risk of hurricanes to potential offshore wind energy infrastructure [5] and the U.S. Transportation Research Board has stated that

* Corresponding author.

| Nomenclature | | | |
|--------------|---|-------------|--|
| c | Component (monopile or tower) | M_p : | plastic moment |
| D | tube diameter | $P_{f,x}$ | Probability of failure given duration x |
| DG | design group | OWT | offshore wind turbine |
| DM | damage measure | R_{max} | percentage of turbines in a WFA lost in the worst storm |
| E | elastic modulus | t | tube thickness |
| EDP | engineering demand parameter | V_{hub} | mean hourly wind speed at hub height |
| F_y | yield stress | WFA | wind farm area |
| H_s | hourly significant wave height | $W_{f,x}$: | mean probability of failure for a WFA given duration x |
| IM | intensity measure | β | lognormal standard deviation |
| L_{20} | : number of turbines failed per WFA in a 20 yr period | θ | median ratio of critical buckling moment to plastic moment |
| M_{cr} | critical buckling moment | λ | slenderness ratio |

existing European technical standards “have deficiencies in their coverage (for example, storms and hurricanes on the Atlantic coast and in the Gulf of Mexico)” [6]. To provide insight into the extent of hurricane risk to offshore wind energy infrastructure, this study first proposes a risk evaluation framework, adapted from a framework in performance-based earthquake engineering. The framework is applied to a hypothetical scenario in which the portions of the nine Atlantic WFAs with water depths less than 40 m are fully populated (i.e., the WFAs are filled with OWTs spaced at 1 km). The portions of the WFAs meeting this depth condition are shown in Fig. 1 and superimposed with a measure of hurricane exposure based on data provided by the National Oceanic and Atmospheric Administration (NOAA) and the NHC [2,4,7].

The quantification of the risk of failure to OWTs exposed to hurricanes is important to financing and insurance of offshore wind energy projects [5,8]. Although a well-established industry for quantifying the risk of natural catastrophes exists [9–11], there is currently no established practice for quantifying the risk of hurricanes to offshore wind energy infrastructure. Quantifying this risk presents several challenges, including a lack of long-term measurements of wind and wave conditions, complexity in modelling spatio-temporal correlations of wind and wave fields generated by hurricanes, lack of test data measuring the structural capacity of full scale OWT components, and the nonlinear structural response of OWTs subjected to hurricane conditions [12]. While there have been some instances in the historical record of onshore wind turbines failing during hurricanes [13,14], no structural damage to OWTs during hurricanes or similar extreme events has so far been observed. This lack of historical performance information necessitates the use of stochastic, numerical models, rather than empirical models, to quantify risk [15,16].

This paper proposes a methodology for estimating the probability of OWT support structure failure due to hurricanes. Here, the support structure is defined as the monopile foundation-tower system that extends from the seafloor to the nacelle. The methodology is based on the Pacific Earthquake Engineering Research Center (PEER) framework for evaluating earthquake risk [17]. The proposed framework is organized into three components: hazard intensity estimation of wind and wave fields during hurricanes, structural response estimation of OWTs during hurricane-induced wind and wave, and fragility estimation of OWTs subjected to axial-flexural loading. Use of the framework is illustrated with a case study in which the likelihood of failure is estimated for approximately 7000 hypothetical OWTs, each with capacity of 5 MW and installed within the portions of the nine WFAs shown in Fig. 1. Considering the wind resource at these sites, these ~7000 OWTs would generate mean power of ~18 GW. This scenario represents the condition when all nine WFAs are developed with

OWTs spaced at 1 km for the portion of their areas with water depths appropriate for monopiles (i.e., water depths less than 40 m). The authors recognize that these wind energy areas will likely be developed with turbines that have rated capacities closer to 8 MW or 12 MW. This study uses the 5 MW benchmark, however, to demonstrate the workings of the proposed risk assessment framework and for consistency with the publicly available National Renewable Energy Laboratory (NREL) 5 MW offshore baseline turbine [18].

The mean lifetime (i.e., 20-year) probability of failure of individual turbines is assessed, as well as the expected number of failures in a 20-year period for each of the nine WFAs and the entire Atlantic coast. These failure probabilities, when combined with measures of consequences of failure, provide the overall risk assessment. This paper does not address the consequences of failure, which include complicated supply chain, market, and economic considerations. Hurricane conditions are estimated for each location based on a 100,000-year catalog of simulated hurricane events [19]. The study considers one turbine support structure topology: the NREL 5 MW offshore baseline wind turbine [18], supported by a tapered tubular tower (with hub height 90 m above mean sea level) and a prismatic monopile. One of three possible archetype geometries for the monopile and tower is assigned to each of the WFAs based on that geometry satisfying design standards [20–24] for every location within the WFA. The environmental conditions for design are assessed at each site, for operational conditions, using hindcast data representing hourly conditions of wind and waves from 1980 to 2013 at over 500 locations along the Atlantic coast [25], and, for 50 year extreme conditions, using the 100,000-year catalog of simulated hurricanes [19,20]. Hurricane-induced wind and wave are estimated from two parametric hurricane models: the Holland model for wind [26] and Young’s model for wave [27]. The Holland model provides the radial profile of wind speed as a function of hurricane parameters and is based on cyclostrophic flow balance within the hurricane pressure field [26]. Young’s model is a spectral model that provides the spatial distribution of the significant wave height as a function of hurricane parameters based on radiative transfer of wind energy [27]. Structural response is simulated in the program FAST version 7 [28] using nonlinear dynamic time history simulations of an elastic structural model with a fixed base subjected to a turbulent wind field and linear irregular waves, including the effects of breaking waves. Slam forces due to breaking waves are included by detecting waves in the irregular wave time history that exceed the steepness limit given by Battjes [29], limiting the wave elevation to the breaking wave height for a particular wave, and then amplifying the acceleration kinematics of these waves within the wave time history to represent slam forces consistent with the Wienke model

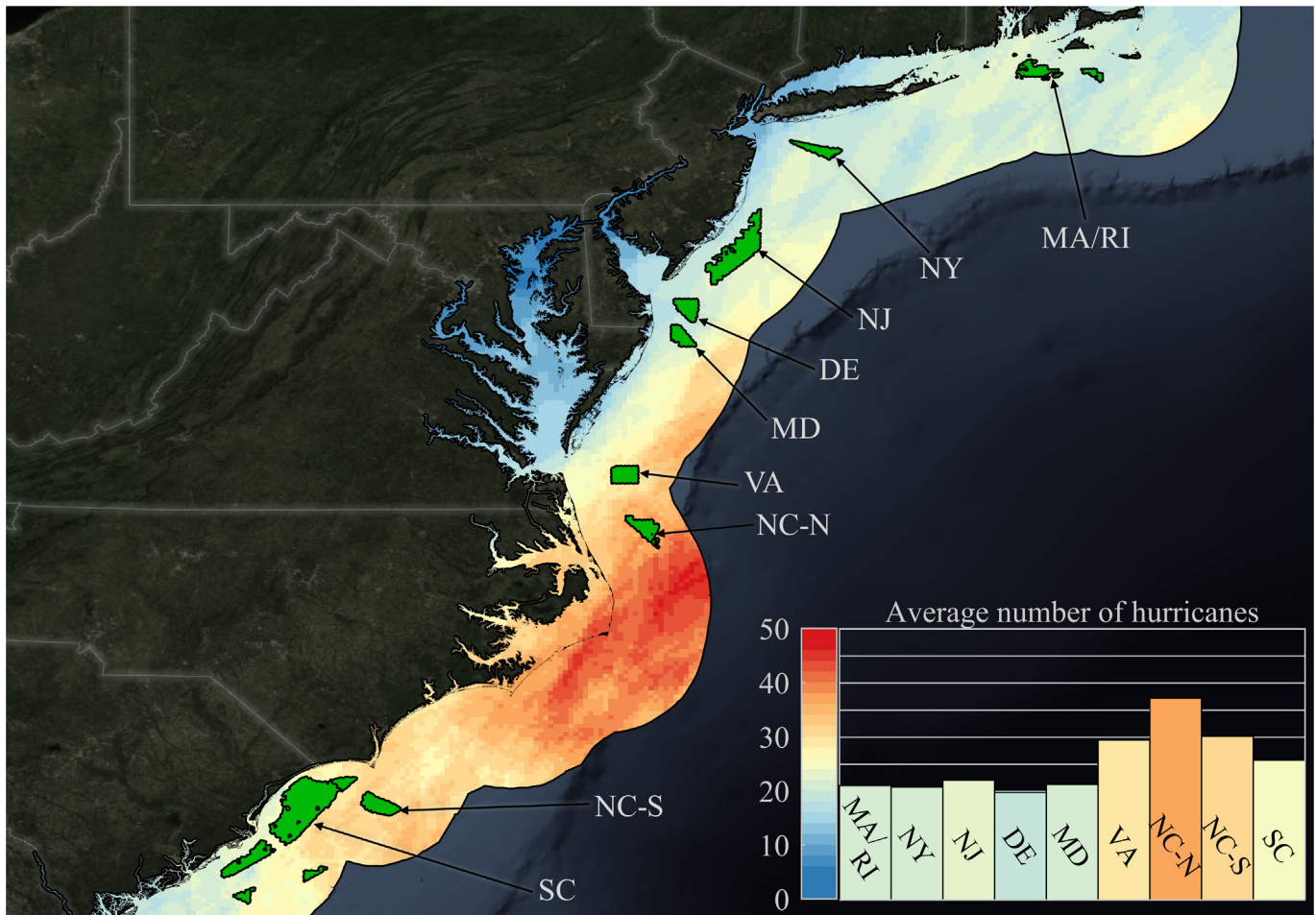


Fig. 1. Locations (green areas) of portions of nine Atlantic WFAs with water depths less than 40 m. The color map and histogram indicate hurricane exposure, defined here as the number of instances, between 1900 and 2013, of hurricane winds (i.e., 33 m/s or greater at 10 m and 1 min averaging time) within 50 km of a particular location [7].

[30], following a method outlined by Hallowell et al. [31]. Failure of the OWT tower and monopile is predicted through a fragility function, based on an analysis of experiments in the literature. The fragilities of other damage states, such as those associated with the blades, mechanical equipment or the seabed, are not considered in this study.

This paper starts with background on relevant prior research on assessing risk to OWTs subjected to hurricanes. Next, a framework for assessing hurricane risk is introduced, followed by a numerical example that is used to both illustrate the proposed framework and to provide meaningful estimates of the risk of hurricanes to wind farms located on the U.S. Atlantic coast. The description of the numerical example starts by defining the nine WFAs in terms of their location, range of water depths, number of turbines, total power generation capacity, and archetype geometry for the tower and monopile. Next, the results of the example are summarized and discussed for the situation when the rotor of the turbine is idling, and the blades are feathered, both with and without a functional yaw control system. Finally, limitations and conclusions of the study are presented along with suggestions for future work.

2. Background

There is no historical record on the performance of OWTs during hurricane-type events, although there is some relevant, but limited, information on the performance of onshore wind turbines during

such events. In particular, four instances of damage have been observed in Asia during Typhoon Jangmi in 2008 in Taiwan [32], Typhoon Saomai in 2006 in Japan [33,34], Typhoon Maemi in 2003 in Japan [13,34], and Typhoon Dujuan in 2003 in China [35]. In Taiwan, one turbine collapsed, and this was attributed to strong winds, insufficient bolt strength, and a lack of quality control during construction [32]. Typhoon Saomai in Japan caused the collapse of five wind turbines due to the loss of control of the pitch and yaw systems combined with rapidly changing wind directions [33]. In Japan, during Typhoon Maemi, three turbines collapsed, and the cause for two of the three turbines was attributed to stress concentrations around the tower access door combined with slippage of the yaw control system, while the third collapsed due to foundation failure [13]. In China, thirteen turbines were damaged, and the damage was attributed to a lack of yaw control after the turbine lost grid power [34,35]. It is important to emphasize that in three of these four instances, failure of the yaw control system contributed to the structural damage.

In addition to the historical record, there are also several relevant analytical studies which aim to quantify the effect of hurricanes on the response of OWT support structures [36–38]. Kim and Manuel have shown that, during hurricane conditions, the yaw of the rotor and the pitch of the blades of an OWT have a significant effect on the bending moment on the tower, with bending moments varying by as much as a factor of three depending on rotor and blade orientation relative to the principal wind direction [39].

This is especially important for hurricane conditions, when the wind direction can shift rapidly [38–40]. Kim and Manuel also developed a framework for hurricane risk assessment of OWTs which allows for the consideration of the spatial distribution of wind and wave fields and time history simulations of turbulent winds and irregular waves [41]. Mardfekri and Gardoni developed a probabilistic framework for the assessment of OWTs subjected to both hurricanes and earthquakes [42,43]. The framework includes soil structure interaction and is applied to a representative turbine located off of the coasts of Texas and California [42]. The application of the framework found that the annual probability of failure of the support structure of an OWT situated in the Gulf of Mexico is 1.5×10^{-3} [42]. Jha et al. showed that the reliability of OWTs designed for different locations in the U.S. varies with the characteristics of the hurricane hazard at the location [44]. Hallowell and Myers found that the reliability of OWTs varies with changing water depth, exposure to breaking waves, and hurricane conditions [36]. Rose et al. quantified the hurricane risk to four hypothetical offshore wind farms located along the U.S. Atlantic and Gulf coasts. For the Gulf coast location, which had the highest risk according to their calculations, Rose et al. calculated a 13% chance that at least one out of 50 turbines in the farm would collapse because of hurricanes during the 20-year life of the farm [45–48].

In summary, there is no historical record for OWT performance when subjected to hurricanes. The performance record of onshore wind turbines is limited, but shows some evidence that damage may be correlated with errors related to the yaw control system. There are several relevant analytical studies, however none of these concurrently considers: site-specific design of the support structure, spatial variability in wind and wave fields appropriate for hurricanes, the effect of changing water depth within a wind farm, the effect of breaking waves, or structural fragility estimation based on relevant structural experiments. The approach presented here includes these effects in a unified framework for assessing hurricane risk to OWTs.

3. Risk framework

The methodology proposed here for assessing the hurricane risk to OWTs follows the same form of the risk framework developed by Pacific Earthquake Engineering Research Center for performance-based earthquake engineering [17,49,50]. This framework is designed to quantify performance for structures subjected to earthquakes, and the form of the framework which is adopted here is expressed as,

$$P_f = \int \int F_{DM}(DM|EDP) f_{EDP}(EDP|\mathbf{IM}) f_{IM}(\mathbf{IM}) dEDP d\mathbf{IM} \quad (1)$$

where P_f represents the probability of damage (or, in this case, failure), $F_{DM}(DM|EDP)$ represents the conditional cumulative probability of a damage measure DM given an engineering demand parameter EDP , $f_{EDP}(EDP|\mathbf{IM})$, represents the conditional probability of an engineering demand parameter EDP given a vector of multiple hazard intensity measures \mathbf{IM} , and $f_{IM}(\mathbf{IM})$ represents the annual probability of occurrence of the hazard intensity measures \mathbf{IM} . An important assumption of the double integral is that the conditional probabilities are independent [50], and, as such, evaluation of the different components of the integral is typically divided into separate analyses of hazard, structural response, and fragility. Treating the different components of the integral separately allows the risk framework to be broken into three components: hazard analysis, structural response analysis, and fragility analysis, and each of these is discussed further below.

4. Hurricane risk quantification

To provide quantitative insight into the risk of damage to OWTs by hurricanes and to provide details for applying the general framework in the previous section to the specific case of OWTs exposed to hurricanes, this section presents an example risk assessment for a hypothetical scenario. In this scenario, the portions of the nine WFAs with water depths less than 40 m (see Fig. 1) are fully developed with thousands of the NREL 5 MW offshore baseline turbine [4,18], each spaced at 1 km and supported by a monopile, which, for simplicity, is modeled as being fixed to the seabed. Although presently the deepest water in which a monopile has been installed is only 35 m [51], there is an expectation that monopiles will be installed in the future in deeper water still. With this in mind, the paper considers all portions of the nine WFAs with water depths less than 40 m, with bathymetric data obtained from the NOAA coastal relief model [52]. As such, this scenario includes 7132 wind turbines, situated in the WFAs from South Carolina to Massachusetts and results in nameplate capacity of 37 GW and a mean power of 18 GW.

The example considers realistic, site-specific geometries for the monopile and tower. For each WFA, one of three archetypical designs for the monopile and tower are used. The archetype designs are determined using IEC and DNV design standards, but with some simplifications to reduce the number of analyses required [20–23]. The geometry of the prismatic monopile is defined by two parameters, the diameter and thickness, and the geometry of the tapered tower is also defined by two parameters, diameter and thickness at the tower bottom, just above the transition piece. At the tower top, just below the rotor hub, the diameter and thickness are fixed at 3.9 m and 19 mm, with linear variation of diameter and thickness between the tower bottom and top [18]. Fig. 2 shows a schematic of the turbine, tower and monopile along with definitions of key terms and dimensions.

A detailed description of the design procedure to determine the three archetype geometries and to associate each of these geometries with one of the nine WFAs is not provided here for brevity, but is detailed by Hallowell [24]. The fatigue design of the monopiles and towers was assumed to be governed by DNV detail [23], and accumulated fatigue damage was assumed to follow the Miner's Rule, with a Goodman correction for mean stress taken into consideration. The fatigue analysis was limited to DLC 1.2 in IEC 6100-3, where the entire operational range of windspeeds of the NREL 5 MW baseline turbine was modeled, using 6, 1-hr time domain simulations in FAST. The accumulated fatigue damage at a given wind speed is normalized by the PDF of hourly windspeed for a given site, and extrapolated to a lifetime of 20 years. It is noted here that, in all cases, a combination of resonance avoidance criteria, drivability requirements on the monopile slenderness (D/t limited to 150), and fatigue controlled the design of the monopile and tower. The fatigue design of the monopiles and towers assumed the fatigue characteristics of DNV detail C1 [23], with fatigue damage accumulation calculated based on Miner's Rule, including the Goodman correction for mean stress. Fatigue conditions are assessed for only one load case (DLC 1.2 in IEC 61400-3) and following the approach prescribed in IEC 61400-3 [20,53,54].

In no case is the design determined by ultimate response during extreme or operational conditions. The three archetypical geometries are identified by a Design Group (DG), each of which is defined in Table 1.

Table 2 shows the mapping between the three DGs and the nine WFAs. The table also provides the range of water depths in the portion of the WFAs considered in this study, the number of turbines installed in each WFA, the corresponding power capacity of each WFA, and the simulated hurricane arrival rate (i.e., the number

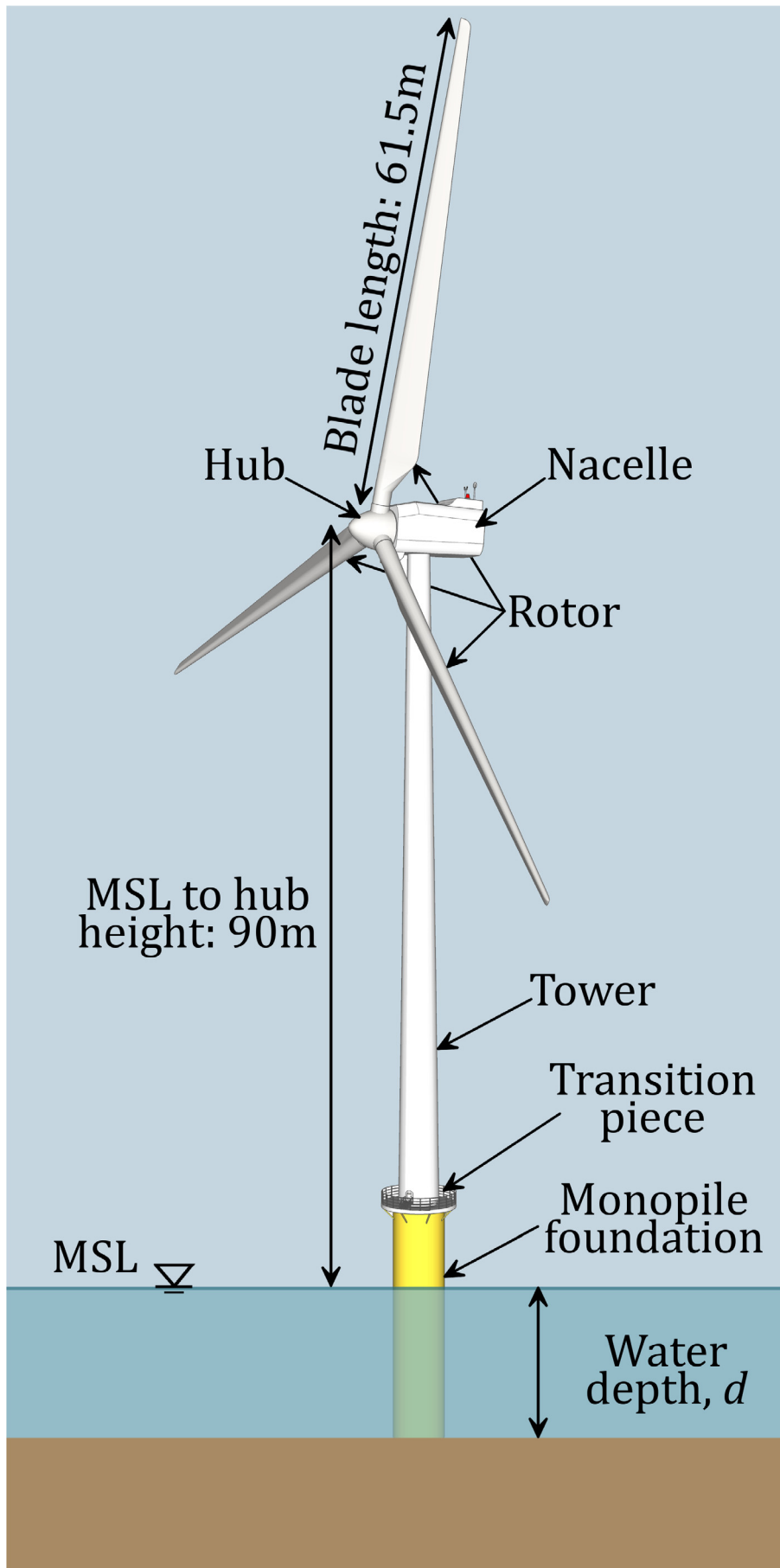


Fig. 2. Schematic including definitions of key terms and dimensions for the tower and monopile supporting the NREL 5 MW offshore baseline turbine. The support structure consists of the tower, transition piece, and monopile.

Table 1
Archetype design group geometries.

| Design group | Monopile | | | Tower bottom | |
|--------------|--------------|----------------|--------------------|--------------|----------------|
| | Diameter (m) | Thickness (cm) | Diameter/Thickness | Diameter (m) | Thickness (cm) |
| A | 6.75 | 4.5 | 150 | 6.50 | 2.0 |
| B | 6.50 | 4.5 | 144 | 6.00 | 2.5 |
| C | 7.00 | 5.0 | 140 | 6.50 | 2.0 |

Table 2
Properties of the nine WFAs considered in this study.

| WFA | Depth Range (m) | # Of Turbines | Total power Capacity (MW) | Hurricane Arrival rate (yr ⁻¹) | DG |
|-------|-----------------|---------------|---------------------------|--|----|
| MA/RI | 28–40 | 428 | 1132 | 0.035 | C |
| NY | 19–40 | 279 | 680 | 0.025 | A |
| NJ | 15–38 | 1223 | 2930 | 0.032 | A |
| DE | 11–32 | 346 | 827 | 0.036 | A |
| MD | 13–40 | 286 | 689 | 0.040 | A |
| VA | 21–37 | 404 | 937 | 0.068 | B |
| NC-N | 27–40 | 394 | 969 | 0.097 | B |
| NC-S | 8–31 | 669 | 1754 | 0.146 | A |
| SC | 6–40 | 3096 | 7865 | 0.126 | A |

of simulated hurricanes causing hurricane strength winds, >33 m/s at 10 m and 1-min averaging time, per year for a given WFA. It is important to recognize that the hurricane arrival rate is influenced by the size of the WFA, as well as its location along the Atlantic coast.

The remainder of this section is organized into four subsections, each of which provides details specific to this example scenario for the individual components of the risk framework specified in Equation (1); specifically, the four subsections provide details on the individual analyses related to hazard $f_{IM}(\mathbf{IM})$, structural response $f_{EDP}(EDP|\mathbf{IM})$, fragility $F_{DM}(DM|EDP)$, and the results of the study P_f .

4.1. Offshore hazard analysis

OWTs subjected to hurricane conditions are loaded by at least two random environmental processes: turbulent winds and irregular waves. As such, the hazard analysis relevant to OWTs exposed to hurricanes should include at least two IMs: one representing the wind and the other representing the waves. Other IMs such as current and storm surge are ignored here. The peak spectral period of the seastate is considered as being normally distributed and conditioned on the wave intensity following the approach in IEC 61400-3 [20], and turbulence is calculated using the Kaimal turbulence model internal to TurbSim, a tool for calculating turbulent wind fields for use in FAST [28,55]. The Kaimal wind turbulence model and associated turbulence intensity may not accurately represent hurricane conditions, however, it is used here because the authors considered it the best model among those implemented in TurbSim and FAST. In this paper, the IM for wind is the hourly mean wind speed at hub height V_{hub} and the IM for wave is the significant wave height H_s . Both IMs and their associated random processes are assumed to be stationary for a period of 1 h.

Estimation of $f_{IM}(\mathbf{IM})$ for wind and wave could be made using statistical extrapolation of measurements, however, since the historical record of hurricane activity is so short (~150 years) and since offshore measurements of wind and wave are so sparse [56], an alternative approach based on a stochastic catalog of simulated hurricane events representing potential hurricane activity for some period of time (typically, tens to hundreds of thousands of years) is used here. Such a catalog characterizes hurricanes with a set of parameters (e.g., eye position, central pressure, maximum wind

speed, radius to maximum wind speed, hurricane translation speed, hurricane translation angle, and the Holland B parameter) defined at regular intervals over the duration of the hurricane. The stochastic catalog is, in effect, a discrete set of realizations of jointly-distributed hurricane parameters calibrated to be consistent with the historical record and understanding of the physics governing hurricanes. This set of realizations must then be somehow transformed to wind and wave IMs. This can be achieved through numerical models, such as ADCIRC/SWAN or MIKE 21 [57,58], which use knowledge of the physical laws governing the atmosphere and ocean to estimate wind and wave during hurricanes. Such models are complex and difficult to implement for the numerical examples presented in this paper which require predictions of wind and wave for thousands of realizations of hurricanes. Instead, a simpler approach is adopted here, based on parametric models to predict wind and wave intensities during hurricanes. In this approach, the relationship between hurricane characteristics and wind and wave IMs is modeled as deterministic, and thus all the variability in the wind and wave conditions comes from the stochastic catalog. The specific stochastic catalog used here is that developed by Liu [19], considering more than 1,000,000 simulated hurricanes representing 100,000 years of potential hurricane activity for the Atlantic Basin. The IM for the gradient wind is estimated using the Holland model [26]. This is then scaled to hub-height using the log-law [59] and to an hourly mean according to Simiu and Scanlan [60], resulting in the IM for wind V_{hub} . The IM for wave H_s is estimated using Young's model [27], which is modified for shallow water depths using the TMA spectrum [61].

4.2. Structural response analysis

The structural response of OWTs subjected to simultaneous wind and wave is nonlinear and influenced by the interaction of aerodynamic, hydrodynamic, structural, operational, and geotechnical effects. In this study, geotechnical effects are ignored by modeling the OWTs with a fixed base at the mudline. Material nonlinear effects due to inelasticity are also neglected because the fragility of the structure is modeled in a way that only requires the results of an elastic analysis (see Section 4.3). As such, the program FAST [28] is used to estimate the function $f(EDP|\mathbf{IM})$. The EDP selected for this study is the maximum compressive stress (from combined bending and axial force actions) acting on the cross-

sections at the base of the monopile and tower. The analyses are conducted on a turbine with an idling rotor, feathered blades, and both a functional and non-functional yaw control system. Consideration of analyses with and without a functional yaw control system is included because of the correlation between control failure and the probability of failure observed in the historical record and analytical literature. The analyses with a functional yaw system consider the OWT with the rotor facing directly into the primary direction of the wind. The analyses with a non-functional yaw control system consider the OWT with the rotor and primary direction of the wind misaligned to give a reasonable representation of the maximum response of the turbine over various yaw angles. Investigations by the authors have found that a yaw error of -35° for the NREL 5 MW offshore baseline turbine is a reasonable representation of the maximum response of the turbine over various yaw angles [24].

The entire catalog of simulated hurricanes contains, in total, millions of hours of storms. This, combined with the thousands of wind turbines considered in this example study, makes structural analysis intractable for every specific combination of V_{hub} and H_s for every turbine and hurricane. Instead, the full set of V_{hub} and H_s for every hour of every hurricane and for every turbine in a DG is reduced to 160 combinations of V_{hub} and H_s that are representative of that DG. This down-sampling is based on the largest empty circle technique [62] and ensures that the 160 combinations sample the envelope of all realized combinations evenly for that particular DG. The result of this process is a set of 160 combinations of V_{hub} and H_s for each of the three DGs. For each DG, structural analyses are conducted for all 160 combinations and for a set of water depths corresponding to the DG, see Tables 1 and 2. The set of water depths includes the minimum and maximum water depths of the DG and intermediate depths spaced at 5 m. This procedure greatly reduces the number of structural analyses required, as analysis results for a specific combination of V_{hub} and H_s and water depth can be readily looked-up and interpolated from a table containing the down-sampled analysis results for a DG.

The process of converting the IMs, V_{hub} and H_s , to EDPs first involves modeling the time series of the turbulent winds and irregular waves. The former is calculated using TurbSim [55] and a Kaimal wind turbulence spectrum, with turbulence intensity and coherence defined in IEC 61400-1 [63] for a Class A turbine, and the latter is calculated with a JONSWAP spectrum [64] modified for shallow water depths using the TMA spectrum [61], following the general method outlined by Agarwal and Manuel for long crested waves [12]. Slam forces due to breaking waves are included by detecting waves in the irregular wave history that exceed the steepness limits given by Battjes [29], limiting the wave elevation to the breaking wave height for a particular wave, and then amplifying the kinematics of these waves to represent slam forces consistent with the Wienke model [30], following a method outlined by Hallowell et al. [31].

The next step in the process of calculating EDPs is to convert the time histories of wind and wave to pressures acting on the surface of the structure. Wind pressures are calculated in FAST using Blade Element Momentum theory [65], and wave pressures are calculated in FAST using the Morison Equation [66]. Coefficients for drag and added mass are modeled equal to 1.0 and structural damping is modeled equal to 1% of critical for the first two fore-aft and side-side modes of the tower [28]. While the structural model considered here is deterministic, the function $f(EDP|IM)$ is modeled as lognormal with variability due to so-called short-term uncertainty in the turbulent wind and irregular wave random processes. Specifically, two sets, one with functional yaw-control and one without, of 24 1-h realizations of the wind and wave processes are

simulated for every structural model considered in this study and for each of the 160 combinations of V_{hub} and H_s relevant to the DG for each structural model. Recall that, although the tower geometry and monopile cross-section are constant for a DG, the monopile length is not, as water depths vary for a DG. As such, for each DG, multiple structural models are created with monopile lengths incremented at 5 m. Response surfaces are created separately for each DG, for the bases of the monopile and tower, for a functional and non-functional yaw control system, and for the range of water depths associated with the DG. These response surfaces are used to create a look-up table for the lognormal mean and standard deviation, which define the lognormal distributions of EDPs for any water depth and combination of V_{hub} and H_s and for any of the three DGs, the two structural components (monopile or tower), or the two yaw control systems states (functional or non-functional).

Since the lognormal mean and standard deviation of the EDP distributions are only defined for a discrete set of water depth and combinations of V_{hub} and H_s , parameters for specific values are calculated with linear interpolation of nearby values. Examples of EDP response surfaces for the monopile for DG = A and water depth = 30 m and for both functional and non-functional yaw control system are provided in Fig. 3, which shows the maximum EDP (shown as black circles for one combination of V_{hub} and H_s) and the mean value (shown as a color map) for the distribution of 24 1-h simulations for all combinations of V_{hub} and H_s relevant to DG = A.

4.3. Fragility analysis

The third component of the risk framework is the analysis of the fragility of the structure, represented with a fragility function $F_{DM}(DM|EDP)$ that defines the probability of failure given an EDP. There are many possible failure states for OWTs subjected to hurricane conditions, including damage related to the blades, mechanical equipment, and the seabed. The scope of the risk assessment considered here is limited to structural failure of the tower or monopile only, and, as such, failure is limited to the exceedance of either the yield stress or a critical stress representing local buckling. For the analyses considered in this case study, an OWT is classified as having failed if either the yield stress or the critical stress is exceeded. As such, all structural models can be reasonably analyzed elastically, since the exceedance of the yield stress will always result in failure and therefore the end of the analysis.

Fragility functions of structural members are commonly represented with a lognormal distribution, and can be derived through a variety of methods [67]. In this research, two fragility functions, one considering local buckling and one considering yielding, are considered and both are estimated through a collection of relevant test data. The two fragility functions are combined to produce a fragility function that represents the probability of failure by either yielding or local buckling. The fragility function representing yielding $F_{DM,yielding}$ is based on a distribution for the yield stress of the steel in the monopile and tower, and, in this case, is modeled with a lognormal distribution with a mean stress $\mu_{F_y} = 386$ MPa and a coefficient of variation $\delta_{F_y} = 5\%$ [16]. This distribution is consistent with the design of the tower or monopile which were based on a material with a 5th-percentile value of the yield stress equal to 350 MPa. The fragility function representing local buckling is developed from a suite of ~130 tests that evaluate the capacity of circular tubes due to bending [68–83]. The test data are shown in Fig. 4.

There are two curves in Fig. 4: one representing the design capacity of a circular tube per DNV-RP-C202 (solid black line) [22] and one representing a modified version of the design capacity curve

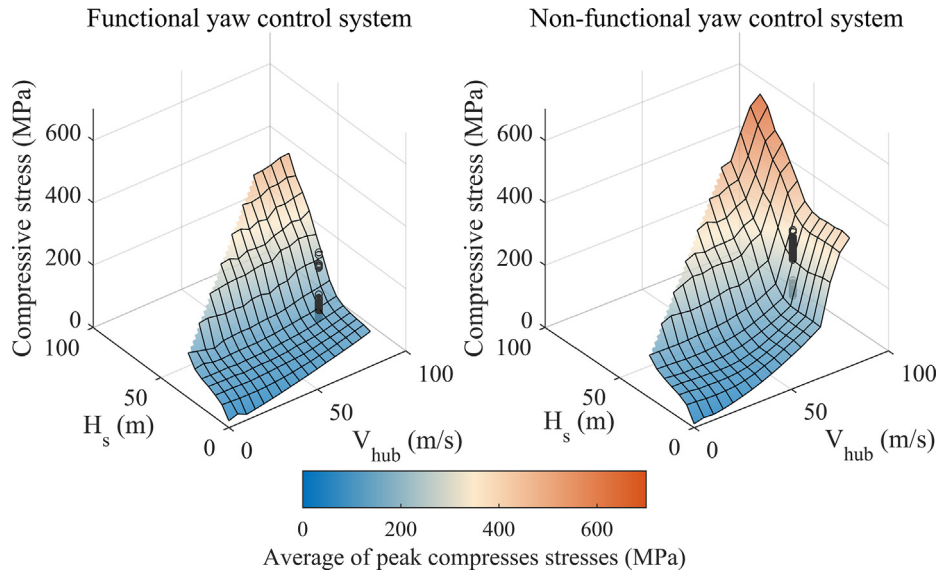


Fig. 3. Example EDP response surfaces for the monopile for DG = A and water depth = 30 m and for a functional yaw control system (left) and a non-functional yaw control system (right). The color map indicates the mean of the distribution of the EDP from 24 1-h simulations for each of the relevant combinations of V_{hub} and H_s , and the black circles represent the maximum compressive stress recorded in each of the 24 simulations for one combination of V_{hub} and H_s .

that has been adjusted to best-fit the data in terms of least-squares (dashed black line). The modified version represents the median ratio of the critical buckling moment to the plastic moment as a

function of section slenderness, $\lambda = \frac{F_y D}{Et}$, where F_y is the yield stress, D is the diameter, E is the elastic modulus, and t is the wall

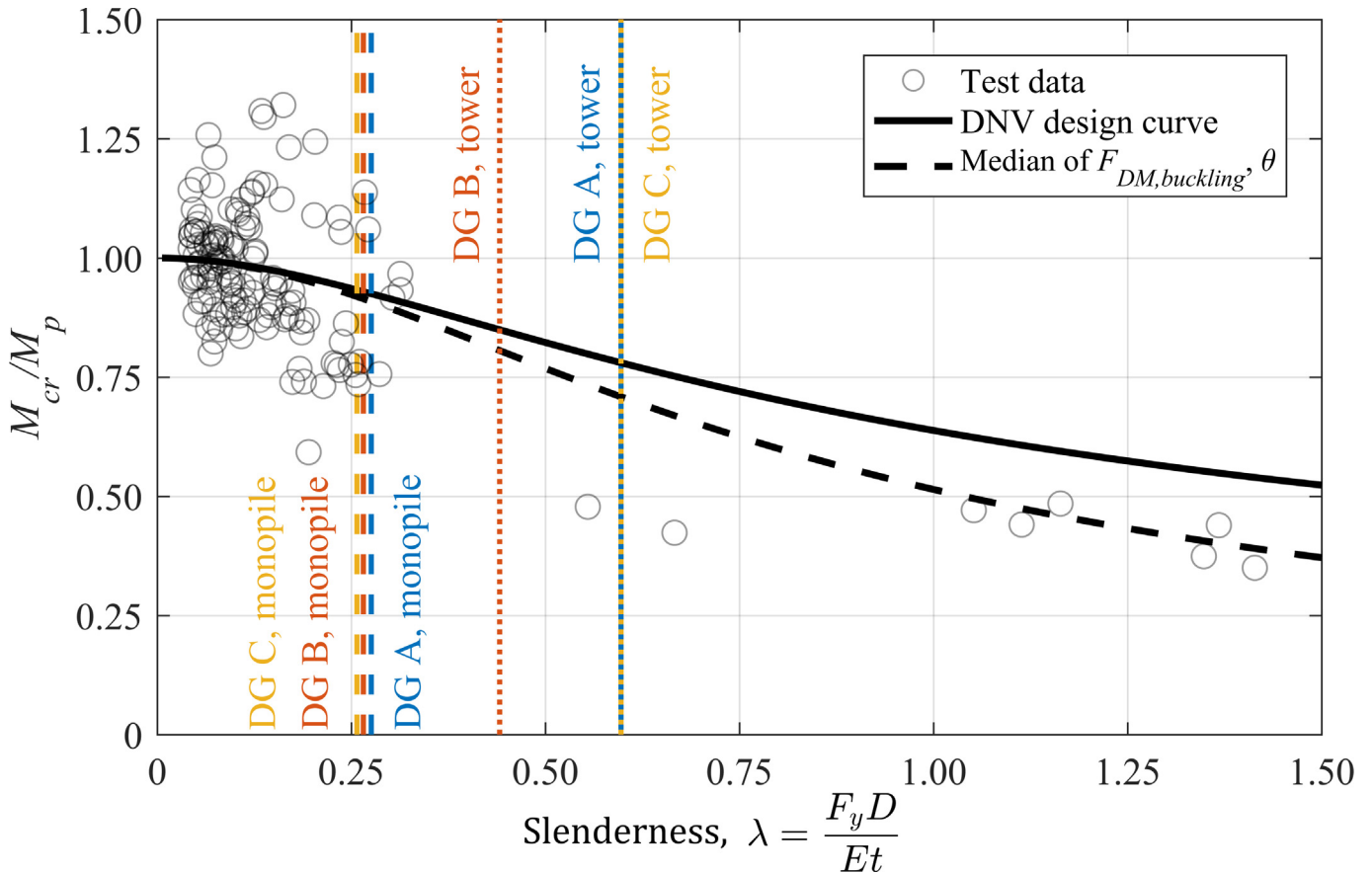


Fig. 4. Test data (black circles) used in the estimation of the buckling fragility function $F_{DM, buckling}$. The solid black curve represents the design capacity per DNV-RP-C202, while the dashed black curve is a modified version of the solid black curve that is adjusted by scaling the coefficient in front of λ^2 in Equation (2) based on least squares regression to the test data. The vertical lines indicate the slenderness of the monopiles and towers given in Table 1. M_{cr} is the critical moment, and M_p is the plastic moment.

thickness. The median ratio θ (dashed black line) is given by,

$$\theta = \frac{M_{cr}}{M_p} = \sqrt{\frac{1}{1 + \frac{25}{9}\lambda^2}} \quad (2)$$

which is the buckling equation in DNV RP-C202, but with the coefficient in front of λ^2 adjusted according to least squares regression of the test data. The fragility function representing elastic/inelastic local buckling $F_{DM,buckling}$ is modeled with a lognormal distribution, with logarithmic standard deviation β equal to,

$$\beta = \sqrt{\frac{1}{n-1} \sum_{i=1}^n \ln\left(\frac{(M_{cr}/M_p)_i}{\theta}\right)^2} \quad (3)$$

where n is the total number of specimens in the test data and $(M_{cr}/M_p)_i/\theta$ is the ratio of the critical moment to the plastic moment for test i divided by the median θ (i.e., the dashed line in Fig. 4) [67]. For

the data in Fig. 4, β is equal to 0.14. The critical moment is converted to a critical stress by dividing the moment by the elastic section modulus for the considered cross-section of the circular tube.

The buckling and yielding fragility functions are combined to represent the probability of failure as a function of EDP,

$$F_{DM}(DM|EDP) = 1 - \left[1 - F_{DM,buckling}(DM|EDP) \right] \left[1 - F_{DM,yielding}(DM|EDP) \right] \quad (4)$$

The resulting fragility functions for the specific archetype monopiles and towers defined in Table 1 are plotted in Fig. 5.

4.4. Estimation of failure probability

Based on the analyses of hazard, structural response, and structural fragility described previously, hurricane risk, expressed here as the probability of structural failure, can be quantified. The procedure for calculating the lifetime (i.e., 20-year) probability of

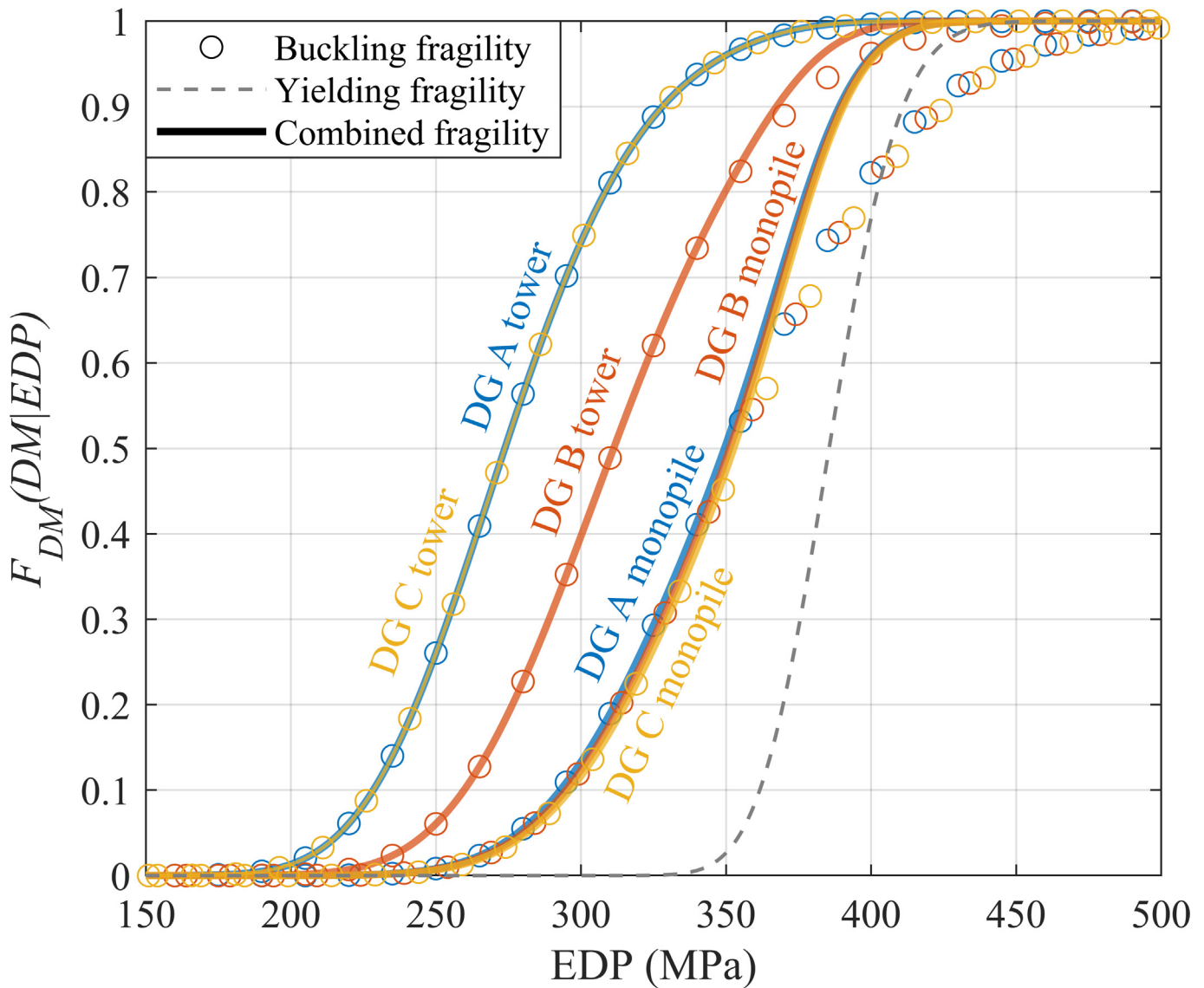


Fig. 5. Fragility functions, combining yielding and inelastic/elastic buckling fragility, for the specific archetype monopiles and towers defined in Table 1. Buckling fragility curves are represented with open markers, with colors representing DG. The yielding fragility curve is indicated with a dashed line, and the combined buckling and yielding fragility curves are indicated with thick colored lines with color indicating the DG.

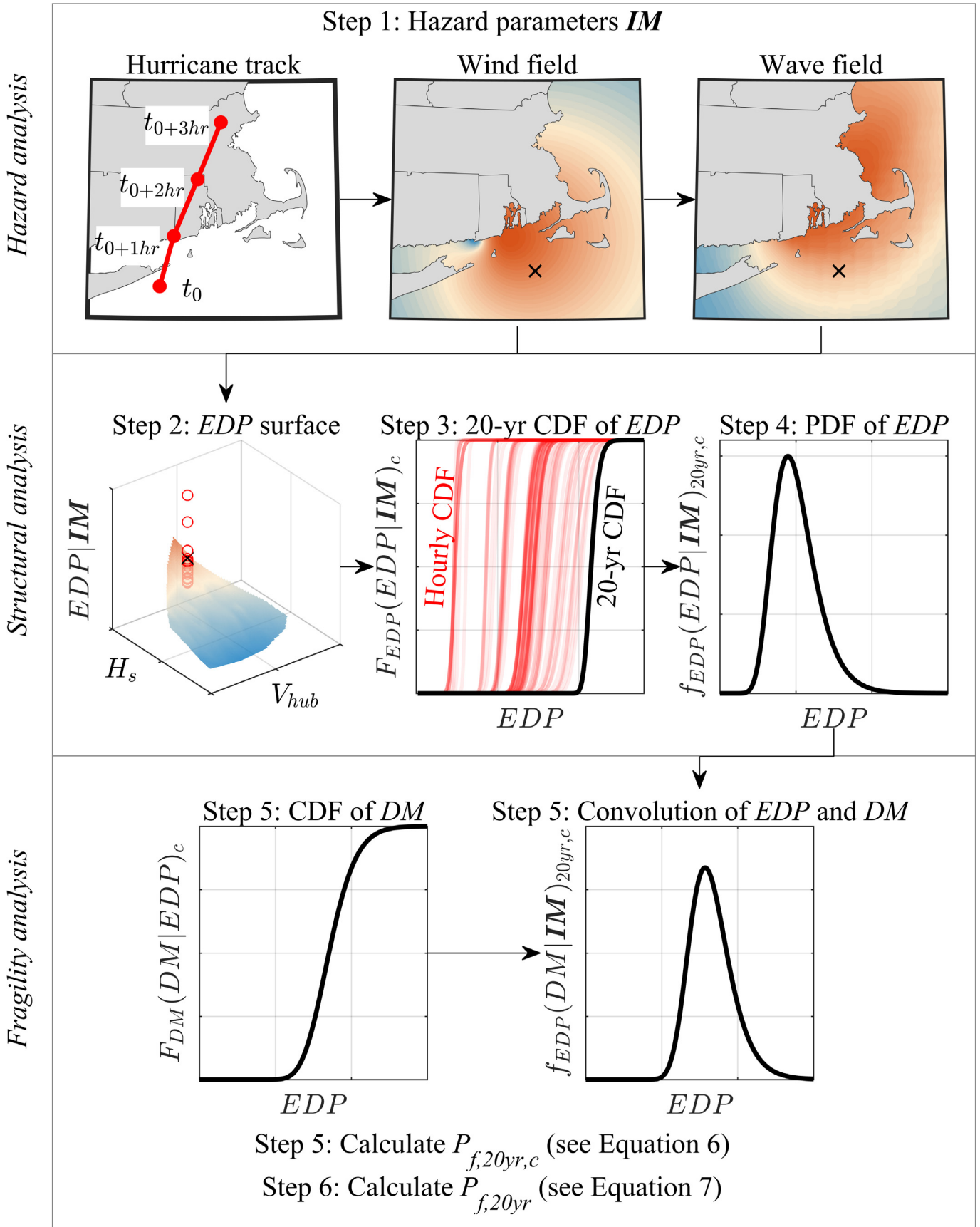


Fig. 6. Flowchart demonstrating the procedure for calculating the lifetime (20-year) probability of failure for both components (tower or monopile) of one OWT for one state of the yaw control system. Note that the EDP surface (Step 2) varies with the OWT, the component, and the state of the yaw control system and the fragility function (Step 5) varies with the component. The probability of failure amongst different OWTs is assumed to be independent.

failure for the support structure (tower and monopile) of one OWT with one state of the yaw control system is shown schematically in Fig. 6 and described below. Subscripts have been added to several of the functions defined previously to clarify the procedure.

1. Calculate V_{hub} and H_s at the location of a particular OWT using the seven hurricane parameters characterizing a hurricane in the simulated catalog for 1 h and the Holland wind field model (for V_{hub}) and Young's model (for H_s) to obtain \mathbf{IM} .
2. For this hourly realization of \mathbf{IM} , determine a corresponding cumulative density function (CDF) for the EDP $F_{EDP}(EDP|\mathbf{IM})_{hr,c}$ based on interpolation of the response surfaces described in Section 4.2. Select the response surface appropriate for the considered OWT component c (tower or monopile) and yaw control system state (functional or non-functional).
3. Repeat steps 1–2 for all hurricane hours in a 20-year period (i.e., a structural lifetime), and, assuming hour to hour independence of $F_{EDP}(EDP|\mathbf{IM})_{hr,c}$, combine the hourly CDFs to obtain the 20-year CDF of the EDP, 20-year

$$F_{EDP}(EDP|\mathbf{IM})_{20yr,c} = \prod_{i=1}^{N_{hrs,20yr}} F_{EDP}(EDP|\mathbf{IM})_{hr,c,i} \quad (5)$$

where $N_{hrs,20yr}$ is the number of simulated hurricane hours i in a 20-year period.

4. Calculate the probability density function $f_{EDP}(EDP|\mathbf{IM})_{20yr,c}$ by differentiating $F_{EDP}(EDP|\mathbf{IM})_{20yr,c}$ with respect to EDP.
5. Convolve $F_{EDP}(EDP|\mathbf{IM})_{20yr,c}$ with $F_{DM}(DM|EDP)_c$ (see Section 4.3) to obtain the lifetime probability of failure $P_{f,20yr,c}$ for a particular turbine and component,

$$P_{f,20yr,c} = \int f_{EDP}(EDP|\mathbf{IM})_{20yr,c} F_{DM}(DM|EDP)_c dEDP \quad (6)$$

Note that both the EDP and DM measures are component specific.

6. Repeat steps 1–5 for both components (tower and monopile), and calculate the 20-year probability of failure of the entire support structure,

$$P_{f,20yr} = 1 - (1 - P_{f,20yr,tower})(1 - P_{f,20yr,monopile}) \quad (7)$$

Equation (7) assumes that the probability of failure of the monopile and tower are independent events, while, in practice, the event of failure is not expected to be totally independent for the monopile and tower.

The result of the above procedure $P_{f,20yr}$ is the lifetime probability of failure for one turbine, one state of the yaw control system, and one 20-year period from the hurricane catalog. The procedure is repeated 5000 times, for each of the 5000 20-year periods in the 100,000-year hurricane catalog. This entire procedure is then repeated for both yaw control system states.

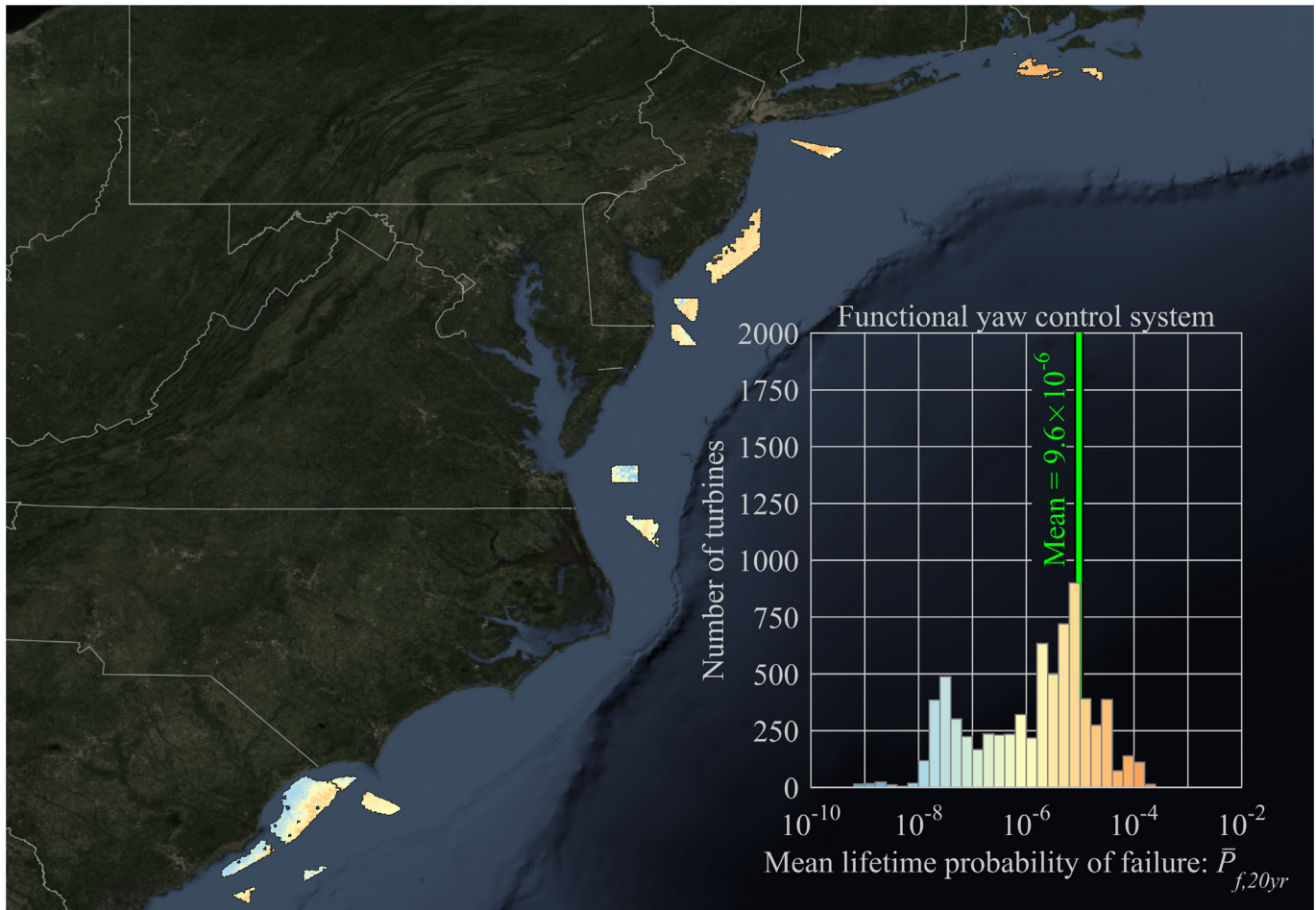


Fig. 7. Mean lifetime probability of failure $\bar{P}_{f,20yr}$ for each of the 7132 turbines in this study for a functional yaw control system.

Two additional measures are derived from $P_{f,20yr}$ to provide alternative metrics for the risk of hurricane-induced failure to OWTs. The first measure is the mean lifetime probability of failure for a particular OWT,

$$\bar{P}_{f,20yr} = \frac{1}{5,000} \sum_{i=1}^{5,000} (P_{f,20yr})_i \quad (8)$$

The second measure is the mean lifetime probability of failure for a WFA,

$$\bar{P}_{f,20yr,WFA} = \frac{1}{N_{turbs,WFA}} \sum_{i=1}^{N_{turbs,WFA}} (\bar{P}_{f,20yr})_i \quad (9)$$

where $N_{turbs,WFA}$ is the number of turbines in a particular WFA. The third measure is the expected number of failures for a WFA in 20 years,

$$\bar{L}_{20yr,WFA} = \frac{1}{5,000} \sum_{j=1}^{5,000} \sum_{i=1}^{N_{turbs,WFA}} (\bar{P}_{f,20yr})_{ij} \quad (10)$$

where $(\bar{P}_{f,20yr})_{ij}$ is the probability of failure in a particular 20-year period j for turbine i located within a particular WFA. The probability of exceedance of the number of turbine failures in 20 years is calculated by omitting the outer summation in Equation (10),

ranking the expected number of failures per WFA from highest to lowest for each 20-year period in the catalog, and then calculating the corresponding probability of exceedance for each 20-year period. The next section provides numerical results for these three measures of risk: $\bar{P}_{f,20yr}$, $\bar{P}_{f,20yr,WFA}$, and $\bar{L}_{20yr,WFA}$.

4.5. Numerical results

The mean lifetime (i.e., 20-year) probabilities of failure for each turbine in this study are given in Figs. 7 and 8, for a functional and non-functional yaw control system, respectively. For a functional yaw control system, the minimum $P_{f,20yr,c}$ of an individual turbine is 7.3×10^{-10} in the DE WFA at a location with a water depth of 31 m, and the maximum is 3.4×10^{-4} in the NJ WFA at a location with a water depth of 27 m. For a non-functional yaw control system, the minimum $P_{f,20yr,c}$ of an OWT is 1.5×10^{-7} in the VA WFA at a location with a water depth of 30 m, and the maximum is 1.6×10^{-3} in the SC WFA at a location with a water depth of 38 m. The mean of $\bar{P}_{f,20yr}$ for all the turbines in the entire Atlantic coast is 9.6×10^{-6} (COV = 229%; median = 2.4×10^{-6}) for functional yaw control and 2.9×10^{-4} (COV = 101%; median = 2.8×10^{-4}) for non-functional yaw control. These individual turbine results are aggregated by WFA, for both a functional and non-functional yaw control system, and presented in Table 3. The probability of exceedance curves for the expected number of failures in 20 years for each WFA (as well as the exceedance curve for all WFAs) are given in Fig. 9.

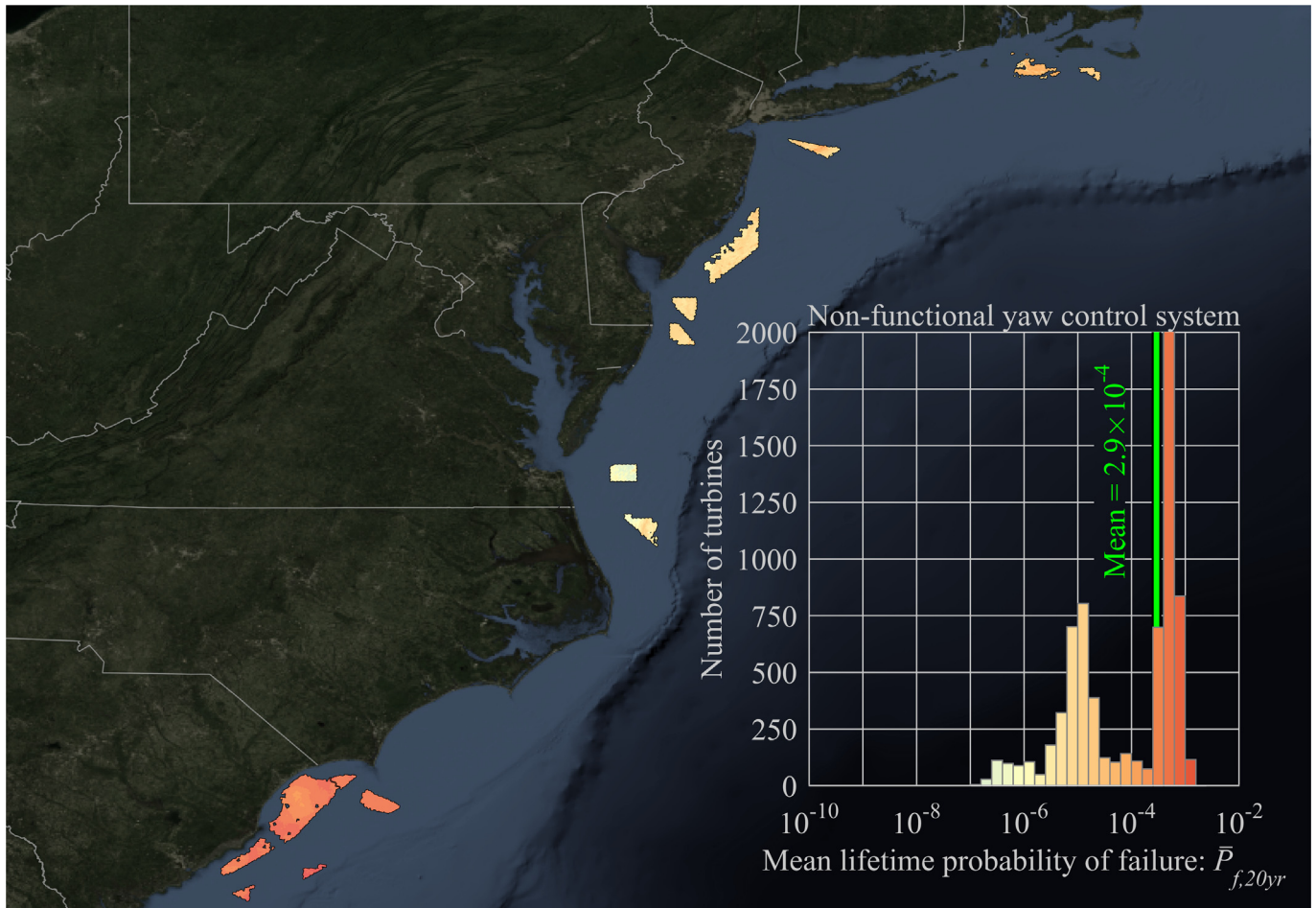


Fig. 8. Mean lifetime probability of failure $\bar{P}_{f,20yr}$ for each of the 7132 turbines in this study for a non-functional yaw control system.

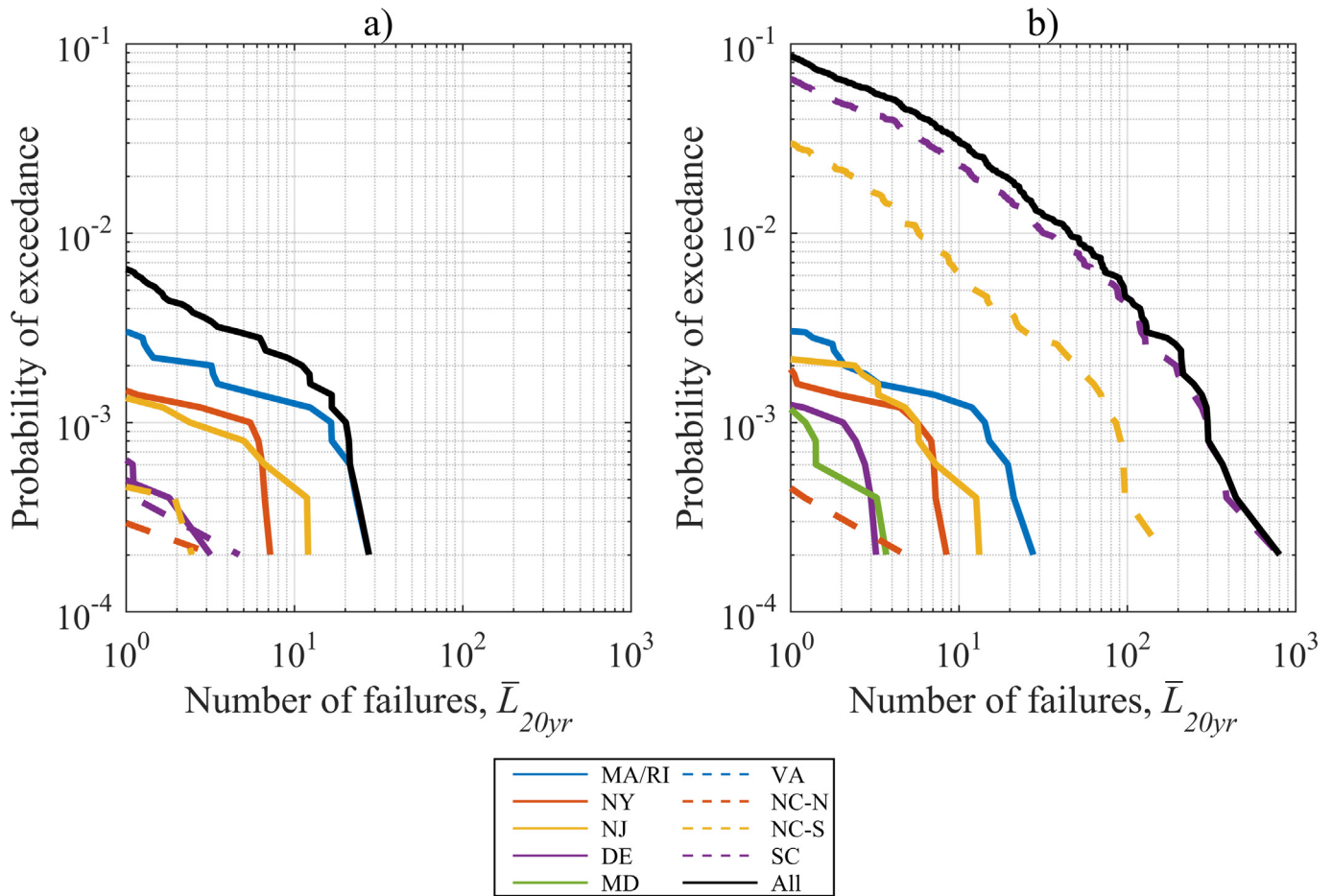


Fig. 9. Probabilities of exceedance for the expected number of failures in 20 years for each for each WFA (a) with and (b) without a functional yaw control system.

Table 3
Results by WFA.

| WFA | Functional yaw control | | Non-functional yaw control | |
|-------|--------------------------------|-------------------------------|--------------------------------|-------------------------------|
| | $\bar{P}_{f,20yr,WFA}$ (Eq. 9) | $\bar{L}_{20yr,WFA}$ (Eq. 10) | $\bar{P}_{f,20yr,WFA}$ (Eq. 9) | $\bar{L}_{20yr,WFA}$ (Eq. 10) |
| MA/RI | 6.7×10^{-5} | 2.9×10^{-2} | 6.4×10^{-5} | 2.7×10^{-2} |
| NY | 2.9×10^{-5} | 8.1×10^{-3} | 3.8×10^{-5} | 1.1×10^{-2} |
| NJ | 1.1×10^{-5} | 1.3×10^{-2} | 1.1×10^{-5} | 1.4×10^{-2} |
| DE | 8.3×10^{-6} | 2.9×10^{-3} | 1.0×10^{-5} | 3.5×10^{-3} |
| MD | 4.0×10^{-6} | 1.1×10^{-3} | 1.3×10^{-5} | 3.7×10^{-3} |
| VA | 5.1×10^{-7} | 2.1×10^{-4} | 1.1×10^{-6} | 4.4×10^{-4} |
| NC-N | 2.3×10^{-6} | 9.1×10^{-4} | 5.7×10^{-6} | 2.3×10^{-3} |
| NC-S | 2.9×10^{-6} | 2.0×10^{-3} | 5.1×10^{-4} | 3.4×10^{-1} |
| SC | 3.5×10^{-6} | 1.1×10^{-2} | 5.4×10^{-4} | 1.7×10^0 |
| All | 9.6×10^{-6} | 6.8×10^{-2} | 2.9×10^{-4} | 2.1×10^0 |

5. Discussion

Overall, the probabilities of failure calculated in this study are relatively low. Recall that none of the structural proportions of the three DGs in this study were controlled by extreme storm conditions; rather, the proportions were controlled by a combination of fatigue demands, constructability requirements and resonance avoidance. As such, the reliability of the designs in terms of extreme storms is expected to be higher than that targeted by the design standard used here (IEC), and the results of this study are consistent with this logic: the mean lifetime probabilities of failure among the nine WFAs, range between 5.1×10^{-7} (reliability β factor = 4.9) at

the VA WFA and 6.7×10^{-5} (reliability β factor = 3.8) at the MA/RI WFA for a functional yaw control system and between 1.1×10^{-6} (reliability β factor = 4.7) at the VA WFA and 5.4×10^{-4} (Reliability β factor = 3.3) at the SC WFA for a non-functional yaw control system. To put these reliabilities in context, API and ISO standards prescribe a target *annual* (not lifetime) probability of failure between 1.0×10^{-5} and 1.0×10^{-3} (reliability β factors = 4.3–3.1) for high consequence (L1) offshore structures and between 1.0×10^{-3} and 1.0×10^{-2} (reliability β factors = 3.1–2.3) for low consequence (L3) offshore structures [84–86]. The difference in failure probabilities between a functional and non-functional yaw control system emphasizes the importance of maintaining yaw control during

extreme storms, a point that has already been emphasized by other researchers [40,45] and that is consistent with historic performance of wind turbines during storms [32–35]. The analyses for the functional and non-functional yaw system are intended to provide some boundaries on the results, with the functional yaw system results intended to represent a best-case control scenario and the non-functional yaw system results intended to represent an expected scenario given loss of yaw control.

The results in the maps in Figs. 7 and 8 highlight the spatial variability in risk of failure (expressed as the lifetime probability of failure) within and among the WFAs. In the presented formulation, the probability of failure of each turbine is assumed to be independent. The figures show how, for a functional yaw control system, the risk is highest for the NY, NJ and MA/RI WFAs and how, for a non-functional yaw control system, the risk is highest for the NC-S and SC WFAs. When the yaw control system is functional, loading from waves becomes relatively more important than loading from wind, and vice versa when the yaw control system is non-functional. As such, the riskiest sites shift from northern WFAs (i.e., NY, NJ and MA/RI) for the functional yaw system case to southern WFAs (NC-S and SC) for the non-functional yaw system case, because the former WFAs are exposed to large hurricane-induced wave forces in relatively deep waters, while the latter WFAs are exposed to large wind forces due to the higher recurrence of hurricane winds (note how, in Table 2, the hurricane arrival rates are highest for the NC-S and SC WFAs). Overall, the variability of the failure probability is influenced by many site-specific factors including the structural design, the yaw control system, the water depth, and the recurrence of wind and waves due to hurricanes. The diameter of the monopile is noted as having an important influence on failure probabilities, as both the structural demands due to wave loading and structural capacities scale nonlinearly with monopile diameter. It is expected that, if design standards for OWTs transitioned to performance-based design, where factors such as the lifetime probability of failure due to hurricanes are considered explicitly in the design process, then hurricane probabilities of failure could be reduced further still without significant additional costs.

The expected number of OWT failures in a 20-year period for a particular WFA are given in Table 3. For a functional yaw control system, the VA WFA has the lowest expected number of failures in 20 years (2.1×10^{-4}), and the MA/RI WFA has the highest (2.9×10^{-2}). For a non-functional yaw control system, the VA WFA has the lowest (4.4×10^{-4}), and the SC WFA has the highest (1.7×10^0). It is noted that these measures reflect both hurricane exposure and WFA size. Along the entire Atlantic coast, it is expected that 0.07 turbines will fail in 20 years for a functional yaw control system, and 2.1 turbines will fail in 20 years for a non-functional yaw control system.

The probability of exceedance curves in Fig. 9 show the likelihood of exceeding a certain number of turbine failures. The probabilities of at least one turbine failure in 20 years range from nearly 0.0% for the MD and VA WFAs to 0.3% at the MA/RI WFA when turbines have a functional yaw control system. Without a functional yaw control system, the probabilities of at least one turbine failure in 20 years range from nearly 0.0% at the VA WFA to 6.5% at the SC WFA. Again, these results are influenced by both hurricane exposure and WFA. The black curves in Fig. 9 represent the probability of exceeding a certain number of turbines failures for all nine of the WFAs considered here. This curve shows that, if yaw control systems are functional (Fig. 9a), there is a 0.65% chance of at least one turbine and a nearly 0.0% chance of at least 100 turbines failing in 20 years. The black curve in Fig. 9a converges to the MA/RI curve, showing that the worst 20-year period for the entire Atlantic coast includes a hurricane that directly hits the MA/RI WFA. Without

functional yaw control systems, there is an 8.6% chance of at least one turbine and a 0.45% chance of at least 100 turbines failing in 20 years. The black curve in Fig. 9b converges to the SC curve, indicating that the worst 20-year period for the entire Atlantic coast includes a hurricane that directly hits SC WFA. Since the probabilities of failure calculated in this study are so low, it is important to recognize that the results are acutely sensitive to the shape of the tails of the distributions of $F_{DM}(DM|EDP)$ and $f_{EDP}(EDP|IM)$.

6. Limitations

The quantification of probabilities of failure of OWTs subjected to hurricanes involves the synthesis of expertise from many disciplines including atmospheric science, ocean engineering, aerodynamics, hydrodynamics, and structural engineering. Because of this complexity, many simplifications are required to make the analyses considered here tractable. This section summarizes some of the most significant simplifications so that the results are interpreted fairly, and the limitations of the study are understood. First, the study considered only one potential failure mode: structural failure at the base of the monopile or the tower due to yielding and/or local buckling under flexural-axial loading. As such, many other potential failure modes are neglected such as blade failure or seabed failure (i.e., geotechnical). Historical data for onshore wind turbines suggest that blade failure is a significant mode of failure, while data for offshore oil and gas structures suggest that seabed failure is also significant. Moreover, this project did not consider failure of subsea cables or the offshore substation. The probabilities of failure of the offshore substation and subsea cables feeding into it are critical metrics for quantifying overall risk to offshore wind farms, as the failure of either could result in significant downtime and lost energy production for an entire wind farm. For this research, the probability of occurrence for a yaw control failure is not included. Inclusion of yaw control failure probabilities would enable the failure probabilities for functional and non-functional cases to be combined for an overall risk metric. Another limitation of this study is that the contribution of winter storms to the probability of failure is neglected. Winter storms are expected to contribute significantly to the overall probability of failure, particularly for WFAs located in the Northeast U.S. where winter storms are known to cause large waves. Inclusion of any of these factors would result in larger probabilities of failure than those presented here. The Kaimal wind turbulence model used in this research is a simplification used to facilitate compatibility between TurbSim and FAST, and actual turbulence intensities for hurricanes may differ from the one used here. Another factor, which, in contrast, would likely result in smaller probabilities of failure, is wind and wave misalignment. In this study, wind and wave were assumed to be aligned, however, in reality, wind and wave are expected to be misaligned significantly during hurricanes [40]. A final factor noted here is that this study considered only monopile foundations, while jackets or gravity base foundations may be the predominant foundation type for the development of the U.S. Atlantic coast.

In addition to the factors listed above that are omitted entirely from the study, the factors which are considered are often analyzed with important simplifications. For example, the flexibility of the seabed [87] and aerodynamic loading on an OWT tower both influence the loading and response of OWTs, but, in this study, the bottom of the monopile is modeled with a fixed boundary condition and aerodynamic tower loading is not considered. Modeling foundation changes the eigenfrequencies of the structure, and therefore the dynamic response of the structure. It is not clear how the changes in dynamics affect the risk profile of the OWTs. In addition, the lognormal mean and standard deviation of the lognormal distributions of $F_{DM}(DM|EDP)$ and $f_{EDP}(EDP|IM)$ are

determined in this study based on experimental data and numerical results that do not sample deep into the tails of the distributions, while probabilities of failure are acutely sensitive to the shapes of the tails of these distributions. Seastates in this study are characterized with a single independent variable, the significant wave height. Other important variables are either modeled as constant (e.g., the spectral shape of the seastate) or as functionally dependent on the significant wave height (e.g., the peak spectral period). The irregular waves and their associated kinematics in this study are modeled with linear wave theory, although it is expected that large hurricane-induced waves will be nonlinear [12]. The effect of breaking waves are included through the use of amplified kinematics embedded into the irregular wave train calculated from the Wienke slam force model [30]. While the Wienke model is recommended by IEC 61400-3 for modeling slam forces, there is lack of guidance on how to include slam forces in a dynamic time history simulation. The Wienke model is a deterministic wave slam model; although Hallowell et al. have found that breaking wave effects are variable [31]. The sources and effects of variability of breaking wave forces are omitted in this research. Despite these limitations and simplifications, the authors believe that the metrics presented in this study represent a defensible estimate of the risk of failure of OWTs exposed to hurricanes.

7. Conclusions

In this study, a complete framework for the quantification of risk of failure of OWTs subjected to extreme hurricanes is developed and applied to a case study considering nine Wind Farm Areas (WFAs) located along the U.S. Atlantic coast. The study includes guidance on estimating offshore intensity measures (IMs), engineering demand parameters (EDPs), and damage measures (DMs). The results of the case study show that site-specific designs and geometries, intensity measures, fragilities, and the ability of the structure to maintain a functional yaw control system during hurricanes influence the risk of OWTs to hurricanes. The WFAs with the highest lifetime (i.e., 20-year) probability of failure when the yaw control system is functional are MA/RI and NY. The WFAs with the highest lifetime probability of failure when the yaw control system is non-functional are NC-S and SC. The mean lifetime failure probability for all turbines in all WFAs is 9.6×10^{-6} for a functional yaw control system, and 2.9×10^{-4} for a non-functional yaw control system. Further work is needed to quantify the influence of foundation flexibility, grid connections, control systems, higher fidelity breaking wave models, and other support structures (gravity based, jacket and floating) on measures of hurricane risk.

Acknowledgements

This material is based upon work supported by the National Science Foundation under Grant Nos. CMMI-1234560, CMMI-1234656, CMMI-1552559, the Massachusetts Clean Energy Center, the University of Massachusetts at Amherst, and Northeastern University. Any opinions, findings, and conclusions expressed in this material are those of the authors and do not necessarily reflect the views of the National Science Foundation or other sponsors.

References

- [1] W. Musial, P. Beiter, P. Schwabe, T. Tian, T. Stehly, P. Spitsen, 2016 offshore wind technologies market report, U.S. Dep. Energy, 2016, p. 131.
- [2] Bureau of Ocean Energy Management (BOEM), Wind Planning Areas (Shapefile), 2017.
- [3] Department of Commerce, National oceanic and atmospheric administration. Tropical cyclone segments occurring within the eastern pacific and North Atlantic ocean basins, 1900–2013 (shapefile), in: NOAA's Ocean Service Office

- for Coastal Management, 2015.
- [4] S. Creed, C. Taylor, Bureau of Ocean energy management (BOEM), Renew. Energy Leas. Areas (shapefile) (2017).
- [5] U.S. Department of Energy, Wind Vision: a New Era for Wind Power in the United States, 2015.
- [6] Transportation Research Board, Committee on offshore wind energy turbine structural and operating safety, in: Structural integrity of offshore wind turbines: Oversight of design, fabrication, and installation, 2011.
- [7] Department of Commerce, National oceanic and atmospheric administration. Tropical cyclone exposure for U.S. Waters within the North Atlantic ocean basin 1900–2013 (shapefile), in: NOAA's Ocean Service Office for Coastal Management, 2015.
- [8] A. Smith, T. Stehly, W. Musial, Offshore Wind Technologies Market Report (NREL/TP-5000-64283), 2015.
- [9] P. Kleindorfer, H. Kunreuther, Challenges facing the insurance industry in managing catastrophic risks, in: K.A. Froot (Ed.), The Financing of Catastrophe Risk, University of Chicago Press, 1999, pp. 149–194.
- [10] T. Maynard, N. Beecroft, S. Gonzalez, L. Restell, Catastrophe modelling and climate change, 2014. <http://www.lloyds.com/~media/Lloyds/Reports/Emerging Risk Reports/CC and modelling template.V6.pdf>.
- [11] M. Lewis, In nature's casino, New York Times Magazine, 2007.
- [12] P. Agarwal, L. Manuel, Incorporating irregular nonlinear waves in coupled simulation and reliability studies of offshore wind turbines, Appl. Ocean Res. 33 (2011) 215–227, <https://doi.org/10.1016/j.apor.2011.02.001>.
- [13] K. Takahara, N. Mekaru, F. Shinjo, T. Ishihara, A. Yamaguchi, S. Matsuura, Damages of wind turbine on Miyakojima island by typhoon Maemi in 2003, in: European Wind Energy Conference & Exhibition, 2003.
- [14] N.-E. Clausen, Design of wind turbines in an area with tropical cyclones, in: Proceedings of the European Wind Energy Conference & Exhibition, 2006.
- [15] S. Márquez-Domínguez, J.D. Sørensen, Fatigue reliability and calibration of fatigue design factors for offshore wind turbines, Energies 5 (2012) 1816–1834, <https://doi.org/10.3390/en5061816>.
- [16] J.D. Sørensen, N.J. Tarp-Johansen, Reliability-based optimization and optimal reliability level of offshore wind turbines, Int. J. Offshore Polar Eng. 15 (2005) 141–146.
- [17] G.G. Deierlein, H. Krawinkler, C.A. Cornell, A framework for performance-based earthquake engineering, in: Proceedings of the 2003 Pacific Conference on Earthquake Engineering, 2003, pp. 140–148, <https://doi.org/10.1061/9780784412121.173>.
- [18] J.M. Jonkman, S. Butterfield, W. Musial, Definition of a 5-MW reference wind turbine for offshore system development (NREL/TP-500-38060), Natl. Renew. Energy Lab., 2009.
- [19] F. Liu, Projections of Future US Design Wind Speeds Due to Climate Change for Estimating Hurricane Losses, Doctoral Dissertation, Clemson University, 2014.
- [20] International Electrotechnical Commission (IEC), IEC 61400-3 Wind Turbines - Part 3: Design Requirements for Offshore Wind Turbines, 2009.
- [21] Det Norske Veritas (DNV), Offshore Standard DNV-os-j101: Design of Offshore Wind Turbine Structures, 2014.
- [22] Det Norske Veritas (DNV), Recommended Practice DNV-RP-C202: Buckling Strength of Shells, 2013.
- [23] Det Norske Veritas (DNV), Recommended Practice DNV-RP-C203: Fatigue Design of Offshore Steel Structures, 2010.
- [24] S.T. Hallowell, A Framework to Assess Hurricane Risk to Offshore Wind Turbines Including Breaking Waves, Doctoral Dissertation, Northeastern University, 2016.
- [25] United States Army Corps of Engineers (USACE), Wave Information Studies (WIS), 2017. <http://wis.usace.army.mil/>.
- [26] G.J. Holland, J.I. Belanger, A. Fritz, A revised model for radial profiles of hurricane winds, Mon. Weather Rev. 138 (2010) 4393–4401, <https://doi.org/10.1175/2010MWR3317.1>.
- [27] I.R. Young, Parametric hurricane wave prediction model, J. Waterw. Port Coast. Ocean Eng. 114 (1988) 637–652, [https://doi.org/10.1061/\(ASCE\)0733-950X\(1988\)114:5\(637\)](https://doi.org/10.1061/(ASCE)0733-950X(1988)114:5(637)).
- [28] J.M. Jonkman, M.L.B. Jr. Fast User's guide NREL/TP-500-38230. 14AD.
- [29] J.A. Battjes, H.W. Groenendijk, Wave height distributions on shallow foreshores, Coast. Eng. 40 (2000) 161–182.
- [30] J. Wienke, H. Oumeraci, Breaking wave impact force on a vertical and inclined slender pile—theoretical and large-scale model investigations, Coast. Eng. 52 (2005) 435–462.
- [31] S. Hallowell, A.T. Myers, S.R. Arwade, Variability of breaking wave characteristics and impact loads on offshore wind turbines supported by monopiles, Wind Energy 19 (2016) 301–312, <https://doi.org/10.1002/we.1833>.
- [32] J.-S. Chou, W.-T. Tu, Failure analysis and risk management of a collapsed large wind turbine tower, Eng. Fail. Anal. 18 (2011) 295–313, <https://doi.org/10.1016/j.engfailanal.2010.09.008>.
- [33] Z.Q. Li, S.J. Chen, H. Ma, T. Feng, Design defect of wind turbine operating in typhoon activity zone, Eng. Fail. Anal. 27 (2013) 165–172, <https://doi.org/10.1016/j.engfailanal.2012.08.013>.
- [34] Z. Zhang, J. Li, P. Zhuge, Failure analysis of large-scale wind power structure under simulated typhoon, Math. Problems Eng. 2014 (2014), <https://doi.org/10.1155/2014/486524>.
- [35] N.-E. Clausen, A. Candelaria, S. Gjerding, S. Hernando, P.B. Nørgård, S. Ott, N.J. Tarp-Johansen, Wind farms in regions exposed to tropical cyclones, in: 2007 European Wind Energy Conference and Exhibition, 2007.
- [36] S. Hallowell, A.T. Myers, Site-specific variability of load extremes of offshore

- wind turbines exposed to hurricane risk and breaking waves, *Wind Energy* 20 (2017) 143–157, <https://doi.org/10.1002/we.1996>.
- [37] V. Valamanesh, A.T. Myers, J.F. Hajjar, S.R. Arwade, Probabilistic modeling of joint hurricane-induced wind and wave hazards to offshore wind farms on the Atlantic coast, in: *Safety, Reliability, Risk and Life-Cycle Performance of Structures and Infrastructures - Proceedings of the 11th International Conference on Structural Safety and Reliability, ICOSAR 2013* 3, 2013, pp. 247–252. <http://www.scopus.com/inward/record.url?eid=2-s2.0-84892413608&partnerID=tZotx3y1>.
- [38] E. Kim, L. Manuel, On the extreme rotor and support structure response of an offshore wind turbine in an evolving hurricane, Paper No. OMAE-2013-11276, in: *Proceedings of the 32nd International Conference on Offshore Mechanics and Arctic Engineering (OMAE)*, Nantes, France, 2013.
- [39] E. Kim, L. Manuel, Hurricane-induced loads on offshore wind turbines with considerations for nacelle yaw and blade pitch control, *Wind Eng.* 38 (2014) 413–423, <https://doi.org/10.1260/0309-524X.38.4.413>.
- [40] K. Wei, S.R. Arwade, A.T. Myers, V. Valamanesh, Directional effects on the reliability of non-axisymmetric support structures for offshore wind turbines under extreme wind and wave loadings, *Eng. Struct.* 106 (2016) 68–79, <https://doi.org/10.1016/j.engstruct.2015.10.016>.
- [41] E. Kim, L. Manuel, A framework for hurricane risk assessment of offshore wind farms, in: *Proceedings, ASME 2012 31st International Conference on Ocean, Offshore and Arctic Engineering*, 2012, pp. 617–622.
- [42] M. Mardfekri, P. Gardoni, Multi-hazard reliability assessment of offshore wind turbines, *Wind Energy* 18 (2015) 1433–1450, <https://doi.org/10.1002/we.1768>.
- [43] M. Mardfekri, P. Gardoni, Probabilistic demand models and fragility estimates for offshore wind turbine support structures, *Eng. Struct.* 52 (2013) 478–487, <https://doi.org/10.1016/j.engstruct.2013.03.016>.
- [44] A. Jha, D.K. Dolan, W. Musial, C. Smith, Offshore wind energy special session: on hurricane risk to offshore wind turbines in US waters, in: *Offshore Technology Conference*, 2010.
- [45] S. Rose, P. Jaramillo, M.J. Small, J. Apt, Quantifying the hurricane catastrophe risk to offshore wind power, *Risk Anal.* 33 (2013) 2126–2141, <https://doi.org/10.1111/risa.12085>.
- [46] S. Rose, P. Jaramillo, M.J. Small, I. Grossmann, J. Apt, Quantifying the hurricane risk to offshore wind turbines: supporting information, *Proc. Natl. Acad. Sci.* 109 (2012) 3247–3252.
- [47] S. Rose, P. Jaramillo, M.J. Small, I. Grossmann, J. Apt, Reply to Powell and Cocke: on the probability of catastrophic damage to offshore wind farms from hurricanes in the US Gulf Coast, *Proc. Natl. Acad. Sci.* 109 (2012) E2193–E2194.
- [48] M.D. Powell, S. Cocke, Hurricane wind fields needed to assess risk to offshore wind farms, *Proc. Natl. Acad. Sci.* 109 (2012) E2192. E2192.
- [49] G.L. Yeo, C.A. Cornell, Stochastic characterization and decision bases under time-dependent aftershock risk in performance-based earthquake engineering, *Pacific Earthquake Engineering Research Center*, 2005.
- [50] H. Krawinkler, E. Miranda, Performance-based earthquake engineering, *Earthq. Eng. Eng. Seismol. Performance-Based Eng.* 9 (2004) 1–9.
- [51] M. Seidel, Substructures for offshore wind turbines - current trends and developments, in: *Festschr. Peter Schaumann*, 2014, pp. 363–368, <https://doi.org/10.2314/GBV:77999762X>.
- [52] D.L. Divins, D. Metzger, National Geophysical Data Center, National Oceanic and Atmospheric Administration, US Department of Commerce, NGDC coastal relief model, 2008 (Last Accessed December 2017), www.ngdc.noaa.gov/mgg/.
- [53] M.A. Miner, Cumulative damage in fatigue, *J. Appl. Mech.* 12 (1945) A159–A164.
- [54] N.E. Dowling, Mean stress effects in stress-life and strain-life fatigue, 2004. SAE Tech. Pap.
- [55] J.M. Jonkman, L. Kilcher, *TurbSim User's guide: version 1.06.00*, Natl. Renew. Energy Lab., 2012.
- [56] V. Valamanesh, A.T. Myers, S.R. Arwade, J.F. Hajjar, E. Hines, W. Pang, Wind-wave prediction equations for probabilistic offshore hurricane hazard analysis, *Nat. Hazards* 83 (2016) 541–562, <https://doi.org/10.1007/s11069-016-2331-z>.
- [57] J.C. Dietrich, S. Tanaka, J.J. Westerink, C.N. Dawson, R.A. Luettich, M. Zijlema, L.H. Holthuijsen, J.M. Smith, L.G. Westerink, H.J. Westerink, Performance of the unstructured-mesh, SWAN+ ADCIRC model in computing hurricane waves and surge, *J. Sci. Comput.* 52 (2012) 468–497.
- [58] DHI, MIKE 21 SW - Spectral Wave Model: Scientific Documentation, 2014.
- [59] T.R. Oke, *Boundary layer climates*, Routledge, 2002.
- [60] E. Simiu, R.H. Scanlan, *Wind effects on structures*, Wiley, 1996.
- [61] S.A. Hughes, *The TMA shallow-water spectrum description and applications*, 1984. No. CERC-TR-84-7. Coast. Eng. Res. Cent. Vicksburg, MS.
- [62] G.T. Toussaint, Computing largest empty circles with location constraints, *Int. J. Parallel Program.* 12 (1983) 347–358.
- [63] International Electrotechnical Commission (IEC), IEC 61400–61401 Wind Turbines—part 3: Design Requirements for Offshore Wind Turbines, 2009.
- [64] K. Hasselmann, T.P. Barnett, E. Bouws, H. Carlson, D.E. Cartwright, K. Enke, J.A. Ewing, H. Gienapp, D.E. Hasselmann, P. Kruseman, A. Meerburg, P. Muller, D.J. Olbers, K. Richter, W. Sell, H. Walden, Measurements of wind wave growth and swell decay during the joint North sea wave project (JONSWAP), *Dtsch. Hydrogr. Z.* 8 (1973) 95.
- [65] J.F. Manwell, J.G. McGowan, A.L. Rogers, *Wind Energy Explained: Theory, Design and Application*, John Wiley & Sons, 2010.
- [66] J.R. Morison, M.P. O'Brien, J.W. Johnson, S.A. Schaaf, The force exerted by surface waves on piles, *J. Petroleum Technol.* 2 (1950) 149–154.
- [67] K. Porter, R. Hamburger, R. Kennedy, Practical development and application of fragility functions, in: *Structural engineering research Frontiers*, 2007, pp. 1–16.
- [68] D.R. Sherman, Tests of circular steel tubes in bending, *ASCE J. Struct. Eng.* 102 (1976) 2181–2185.
- [69] D.R. Sherman, in: M.N. Pavlovic (Ed.), *Inelastic flexural buckling of cylinders. Steel structures: recent research advances and their applications to design*, Elsevier Applied Science Publishers, 1986, pp. 339–357.
- [70] C.G. Schilling, Buckling strength of circular tubes, *J. Struct. Div.* 91 (1965) 325–348.
- [71] J.O. Jirsa, F.H. Lee, J.C. Wilhoit Jr., J.E. Merwin, et al., Ovaling of pipelines under pure bending, *Offshore Technol. Conf.* (1972).
- [72] M. Elchalakani, X.L. Zhao, R. Grzebieta, Bending tests to determine slenderness limits for cold-formed circular hollow sections, *J. Constr. Steel Res.* 58 (2002) 1407–1430.
- [73] M. Elchalakani, X.-L. Zhao, R. Grzebieta, Cyclic bending tests to determine fully ductile section slenderness limits for cold-formed circular hollow sections, *J. Struct. Eng.* 130 (2004) 1001–1010.
- [74] M. Elchalakani, X.-L. Zhao, R. Grzebieta, Variable amplitude cyclic pure bending tests to determine fully ductile section slenderness limits for cold-formed CHS, *Eng. Struct.* 28 (2006) 1223–1235.
- [75] H. Jiao, X.-L. Zhao, Section slenderness limits of very high strength circular steel tubes in bending, *Thin-Walled Struct.* 42 (2004) 1257–1271.
- [76] M.J. Stephens, G.L. Kulak, C.J. Montgomery, *Local Buckling of Thin-walled Tubular Steel Members*, Thesis Report, University of Alberta, 1982.
- [77] G. Kiyamaz, Strength and stability criteria for thin-walled stainless steel circular hollow section members under bending, *Thin-Walled Struct.* 43 (2005) 1534–1549.
- [78] L. Guo, S. Yang, H. Jiao, Behavior of thin-walled circular hollow section tubes subjected to bending, *Thin-Walled Struct.* 73 (2013) 281–289.
- [79] S. Poonaya, U. Teeboonma, C. Thinwongpituk, Plastic collapse analysis of thin-walled circular tubes subjected to bending, *Thin-Walled Struct.* 47 (2009) 637–645.
- [80] S.J. Fulmer, M.J. Kowalsky, J.M. Nau, T. Hassan, Reversed cyclic flexural behavior of spiral DSAW and single seam ERW steel pipe piles, *J. Struct. Eng.* 138 (2011) 1099–1109.
- [81] N.B. Pueppke, *Buckling Behavior of Spirally Welded Steel Tubes*, Masters Thesis, TU Delft, 2014.
- [82] R.M. Korol, Inelastic buckling of circular tubes in bending, *J. Eng. Mech. Div.* 104 (1978) 939–950.
- [83] P. Seide, V.I. Weingarten, E.J. Morgan, *The Development of Design Criteria for Elastic Stability of Thin Shell Structures*, Technical Report, TRW Space Technology Labs Los Angeles, CA, 1960.
- [84] American Petroleum Institute (API), *API RP2A Recommended Practice for Planning, Designing and Constructing Fixed Offshore Platforms-load and Resistance Factor Design*, 1993.
- [85] A. Younan, F. Puskar, *API RP2EQ-seismic design procedures and criteria for offshore structures*, in: *Offshore Technology Conference*, 2010.
- [86] G.A. Ghoneim, Arctic standards-a comparison and gap study, in: *OTC Arct. Technology Conference*, 2011.
- [87] A.T. Myers, S.R. Arwade, V. Valamanesh, S. Hallowell, W. Carswell, Strength, stiffness, resonance and the design of offshore wind turbine monopiles, *Eng. Struct.* 100 (2015), <https://doi.org/10.1016/j.engstruct.2015.06.021>.